Molecular Dynamics Simulations of Propane in Slit Shaped Silica Nano-Pores: Direct Comparison with Quasielastic Neutron Scattering Experiments

Siddharth Gautam[1*], Thu Le[2], Alberto Striolo[2], David Cole[1]

[1]School of Earth Sciences, The Ohio State University, 275 Mendenhall Laboratory, 125 S Oval Mall, Columbus 43210, OH, United States of America

[2]Department of Chemical Engineering, University College London, London WC1E 6BT, United Kingdom

*Corresponding author email: gautam.25@osu.edu; Phone: (+1) 614-292-7365

Address: School of Earth Sciences, The Ohio State University, 275 Mendenhall Laboratory, 125 S Oval Mall, Columbus, Ohio, 43210, USA

Abstract

Molecular motion under confinement has important implications for a variety of applications including gas recovery and catalysis. Propane confined in mesoporous silica aerogel as studied using quasielastic neutron scattering (QENS) showed anomalous pressure dependence in its diffusion coefficient (J. Phys. Chem. C 119 (2015) 18188). Molecular dynamics (MD) simulations are often employed to complement the information obtained from QENS experiments. Here, we report an MD simulation study to probe the anomalous pressure dependence of propane diffusion in silica aerogel. Comparison is attempted based on the self-diffusion coefficients and on the time scales of the decay of the simulated intermediate scattering functions. While the self-diffusion coefficients obtained from the simulated mean squared displacement profiles do not exhibit the anomalous pressure dependence observed in the experiments, the time scales of the decay of the intermediate scattering functions calculated from the simulation data match the corresponding quantities obtained in the QENS experiment and thus confirm the anomalous pressure dependence of the diffusion coefficient. The origin of the anomaly in pressure dependence lies in the presence of an adsorbed layer of propane molecules that seems to dominate the confined propane dynamics at low pressure, thereby lowering the diffusion coefficient. Further, time scales for rotational motion obtained from the simulations explain the absence of rotational contribution to the QENS spectra in the experiments. In particular, the rotational motion of the simulated propane molecules is found to exhibit large angular jumps at lower pressure. The present MD simulation work thus reveals important new insights into the origin of anomalous pressure dependence of propane diffusivity in silica mesopores and supplements the information obtained experimentally by QENS data.

1. Introduction

Molecular motion under confinement is an interesting topic of research as it entails a variety of peculiar phenomena[1-18]. Anomalous size and loading dependence of molecular dynamics of confined fluids in porous media have been reported[6-8], suggesting the need of better understanding how confinement affects not only the structure but also the transport-properties of confined fluids. Apart from a fundamental interest, a study of molecular motion in confinement is important because it promises to enhance our understanding of industrial processes that depend on confined fluids, for example, catalysis, gas separation and recovery of subsurface gases[1-3] all depend on the ability of fluids to migrate through porous media. Porous materials are classified on the basis of pore sizes[19] into microporous, with pore size less than or equal to 2 nm, mesoporous, with pore size between 2 and 50 nm; and macroporous, with pore size larger than 50 nm. The behavior of fluids confined within micropores stems from a strict geometrical confinement that can put a severe restriction on the degrees of freedom of the confined molecule along the direction of confinement. The behavior of meso-confined fluids, on the other hand, can be thought of as an overlap of approaching fluid substrate interfacial structures[20]. In larger meso-pores the confined fluid may even exhibit interfacial and bulk like properties simultaneously[21].

Although much is known about the loading dependence of the diffusive motion of micro-confined fluids[6,7], studies addressing loading dependence of meso-confined fluids have been relatively scarce. The few studies on this topic reveal interesting and sometimes anomalous loading dependencies. For example, methane confined in carbon aerogel has been found to exhibit a maximum in the diffusion coefficient as a function of loading[22]. In a quasielastic neutron scattering (QENS) study of propane confined in mesoporous silica aerogel, propane diffusion was enhanced at higher loading[23]. It was also found that a relatively large amount of propane molecules were almost immobile at low loadings.

QENS provides spatio-temporal information on the stochastic motion of molecules[24]. It is often complemented by molecular dynamics (MD) simulations[25-33]. Self-diffusion coefficients obtained from MD simulations can be compared directly with those obtained from QENS experiments. In addition, molecular trajectories obtained from simulations provide the opportunity to go a step further by directly calculating quantities that are related to those measured in the experiments. For example, intermediate scattering functions, which are the

inverse Fourier transforms of the dynamic structure factor that can be obtained from a QENS experiment, can be calculated from the simulated molecular trajectories[25-32]. Moreover, given the ability to calculate functions from distinct molecular species separately, MD simulations provide an opportunity to obtain information inaccessible to experiments, and can thus aid in the interpretation of experimental data. This paper stems from the hypothesis that these intermediate scattering functions provide a direct link between experiments and simulation.

We report here a direct comparison of MD simulation of propane in a slit-shaped mesopore obtained from silica solid substrates against QENS experiments on propane in mesoporous silica aerogel that show anomalous loading dependence of propane diffusion. Decay rates of the intermediate scattering functions corresponding to the translation motion of propane calculated from the simulations are compared with the spectral quasielastic widths obtained from the experiment yielding a semi-quantitative agreement and therefore validating the simulation using the experimental data. Building on this validation, various structural and dynamical properties are calculated to aid and explain the experimental observations. Following this approach we show here that simulation data reveal important new insights into the origin of the anomalous pressure dependence of diffusivity observed in the experiments.

The manuscript is organized as follows. After describing the simulation details in section 2, we discuss the validation of the simulation in section 3. Structural information is provided in section 4. More information on the translational and rotational motion of propane is provided in section 5, after which we summarize our concluding remarks in section 6.

2. Simulation details

2.1 Silica model

The QENS experiments were conducted in mesoporous silica aerogels of pore size 15-20 nm. In pores of such size it is expected, based on prior simulation results, that the interface between the solid substrate and the confined fluid is responsible for deviations in the fluid behavior compared to bulk observations[34,35]. To quantify the molecular-level interactions at the interface between solid and fluid it is possible to simulate the fluids confined in slit-shaped pores of width large enough that one solid-fluid interface does not interfere with the other solid-fluid interface across

the pore volume. The pores considered in the present work were of width 20 nm. The geometry of the pores in silica aerogels is approximately cylindrical, thus it is an approximation to describe the pores as slit-shaped in our simulations. However at the molecular –level, it is expected that the curvature of the experimental substrates is much lower than the propane molecular size, and therefore a flat solid-fluid interface is considered a reasonable approximation for the simulation system. Finally, the silica aerogel is an amorphous material. However, because propane-silica interactions are not expected to be dominated by preferential interactions such as hydrogen bonds, we expect that the atomic-structure of the solid substrate is not an important parameter in dictating solid-propane interactions provided that the atomic density of the solid substrate is comparable to that of the experimental substrate. Building on out prior research the silica model used in this work was obtained by cutting the β-cristobalite SiO_2 crystal along the (1 1 1) crystallographic face. A detailed description of the solid morphology has been provided elsewhere[36, 37]. The simulation box dimensions were 4.37×4.79×23.3 nm^3. Because of periodic boundary conditions, the system considered is composed by SiO_2 slabs that are infinitely long along the X and Y directions, and separated along the Z direction by the slit-shaped pore. The solid substrate bears no net charge, and all the non-bridging O atoms on the pore surfaces are fully protonated, yielding a high density of surface –OH groups. Figure 1 shows the solid substrate from different coordinate planes and Figure 2 gives a sample snapshot of the simulated system at 337 K and at pressures of 8 and 58 bar, respectively.

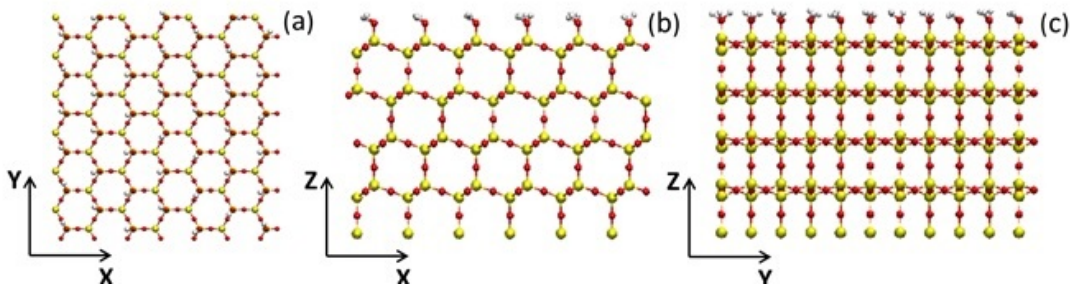

Figure 1. Models of the hydroxylated β-cristobalite SiO_2 crystal along different axis. (a) OH-terminated silica surfaces; only the upper 2 atomic layers are shown for clarity. (b), (c) Side views of silica slabs along X-Z and Y-Z axis, respectively. Red spheres are O, white is H, and yellow is Si.

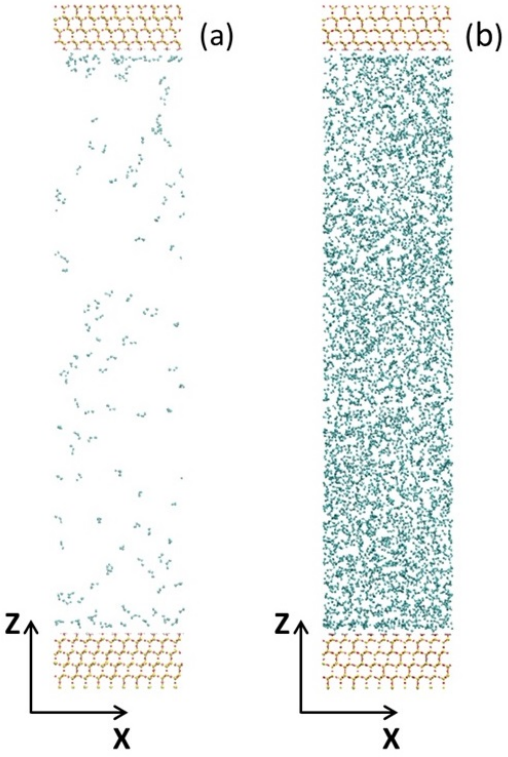

Figure 2. Representative snapshot of the simulation box consisting of (a) 127 propane molecules at T = 337 K and P = 8 bar and (b) 2305 propane molecules at T = 337 K and P = 58 bar within a 20 nm silica slit pore. The solid silica slabs are continuous along both X and Y directions. No bulk region exists. The color scheme is the same as that used in **Figure 1** for the solid substrate. Propane molecules are shown in cyan, with each sphere representing either a CH_2 or CH_3 group.

2.2 Molecular models

Propane molecules are modeled using the TraPPE-UA force field.[38] In this force-field, methyl (CH_3) and ethyl (CH_2) groups are treated within the united-atom formalism. The bond lengths are fixed while the CH_3-CH_2-CH_3 angle undergoes bending motion constrained by a harmonic potential. The total system energy is obtained as the sum of dispersive (van der Waals), electrostatic, bond length and angle interactions:

$$E_{total} = E_{VDW} + E_{bond\ stretch} + E_{electrostatic} + E_{angle\ bend} \quad (1)$$

E_{VDW} and $E_{\mathrm{electrostatic}}$ are expressed by 12-6 Lennard-Jones and Coulombic potentials, respectively. Lennard-Jones parameters for non-like components were obtained using Lorentz-Berthelot mixing rules[39-41]. The CLAYFF force field[42] was implemented to simulate the silica substrate. The hydrocarbon does not bear partial charges. All atoms on the solid silica, except for

H of the surface –OH groups, remain rigid throughout the whole length of the simulations. The O-H bond is allowed to move (flexible bond length and orientation) with a harmonic potential. The potential cutoff was set at 1.4 nm in accordance with the TraPPE-UA force field, with no long range correction applied.

2.3 Simulation methodology

First, Gibbs ensemble Monte Carlo (GEMC) simulations were conducted to determine the equilibrium configurations and densities of the absorbed propane phase within the silica pore at T = 337 K and P = 8 and 58 bars, conditions which mimic the experimental studies. For each simulation, 3375 propane molecules were initially placed in a bulk phase, at a desired pressure, which is set to be in equilibrium with the pore phase that consists of empty silica pore (no confined propane). Molecular exchanges of propane between the two phases were allowed to occur for 2×10^6 moves during equilibration, after which the production phases were initiated and the averages were analyzed for 1×10^6 moves. Equilibration was considered achieved based on chemical potential equality for the bulk phase and the confined phase.

Next, MD simulations were carried out to investigate the kinetic properties of the systems using as initial configurations the equilibrated ensembles from the GEMC simulations. In the QENS experiment, a monolithic sample that fit tightly in the sample cell was used. As a result the contribution of fluid not adsorbed in the pores to the spectra was less than 10%. To achieve consistent comparison, only the contribution from propane molecules simulated inside the pore was considered for the data analysis discussed below. This corresponded to 2305 propane molecules at 58 bar and 127 molecules at 8 bar. All MD simulations were carried out within orthorhombic simulation boxes in the NVT ensemble with periodic boundary conditions. Temperatures of silica and fluid were controlled separately by two Nosé-Hoover thermostats[43, 44] with relaxation times of 200 fs each. Corrections for long-range electrostatic interactions were taken into account by the particle-mesh Ewald summation[45]. The MD simulations were conducted using the Groningen Machine for Chemical Simulations (GROMACS) simulation package, version 5.0.4[46, 47]. The leapfrog algorithm[48] with time steps of 1 fs was implemented to integrate the equations of motion. Simulations were conducted for 50 ns for all systems investigated. MD simulations at the temperature of 365 K were carried out by heating the configurations at 337 K while keeping the number of molecules fixed. This is consistent with the

experimental procedure, wherein the temperature was raised while the sample was isolated and exchanged no propane molecules with the environment. Data analysis was carried out over the final 1 ns trajectories of each MD simulation.

3. Validation of the simulation with QENS data

In a QENS experiment on a hydrogen bearing sample, the measured signal is proportional to the incoherent dynamic structure factor $S_{inc}(Q,\omega)$ where $\hbar Q=|\hbar \boldsymbol{Q}|$ and $\hbar\omega$ are, respectively, the momentum and energy transferred between the sample and the scattered neutron in the scattering event and $\hbar$ is the reduced Planck constant. This quantity contains spatio-temporal information on the sample by virtue of its dependence on space and time. In general this quantity consists of two parts – an elastic component and a quasielastic component. Thus one can write,

$$S_{inc}(Q,\omega) = A(Q)\delta(\omega) + [1 - A(Q)]f(Q,\omega) \qquad (2)$$

In Eq. (2), the first term on the right hand side is the elastic contribution and the second term is the quasielastic contribution. The prefactor $A(Q)$ gives the fraction of total scattering that is elastic and is therefore called elastic incoherent structure factor (*EISF*). The quasielastic broadening is represented by the function $f(Q,\omega)$. In case of diffusive motion, this function has a Lorentzian profile, which, ignoring a constant multiplier, can be given as

$$f(Q,\omega) = L(\Gamma(Q),\omega) = \frac{\Gamma(Q)}{(\Gamma^2(Q)+4\omega^2)} \qquad (3)$$

where $\Gamma(Q)$ is the half-width at half-maximum of the peak profile.

In the QENS measurements in Ref. 23, the QENS signal was fitted with a model $S_{inc}(Q,\omega)$ convoluted with instrument resolution. The model $S_{inc}(Q,\omega)$ combined Eq. 2 with Eq. 3 plus an addition term that accounted for the background, yielding.

$$S_{inc}(Q,\omega) = \{A(Q)\delta(\omega) + [1 - A(Q)]L(\Gamma(Q),\omega) + B(Q,\omega)\} \otimes R(Q,\omega) \qquad (4)$$

Representative experimental spectra at two pressures fitted with Eq. 4 are shown in Figure 3. It can be seen that the Lorentzian component of the fit at higher pressure is broader, indicating a faster diffusion. Also, the relative contribution of the elastic component shown by blue dotted line can be seen to be lower at higher pressure, which means a lower value of $A(Q)$ at high

pressure. The fitting parameters, $A(Q)$ and $\Gamma(Q)$ obtained by fitting the experimental spectra with Eq. 4 were analyzed further. For a given pressure, the values of $A(Q)$ obtained from the fits were found to be constant in Q. This indicated the presence of molecules that were immobile on the time scales accessible to the instrument. Further, it indicated that the contribution to the QENS signal came from translational diffusion and not from a localized motion like rotation or two-site jump.

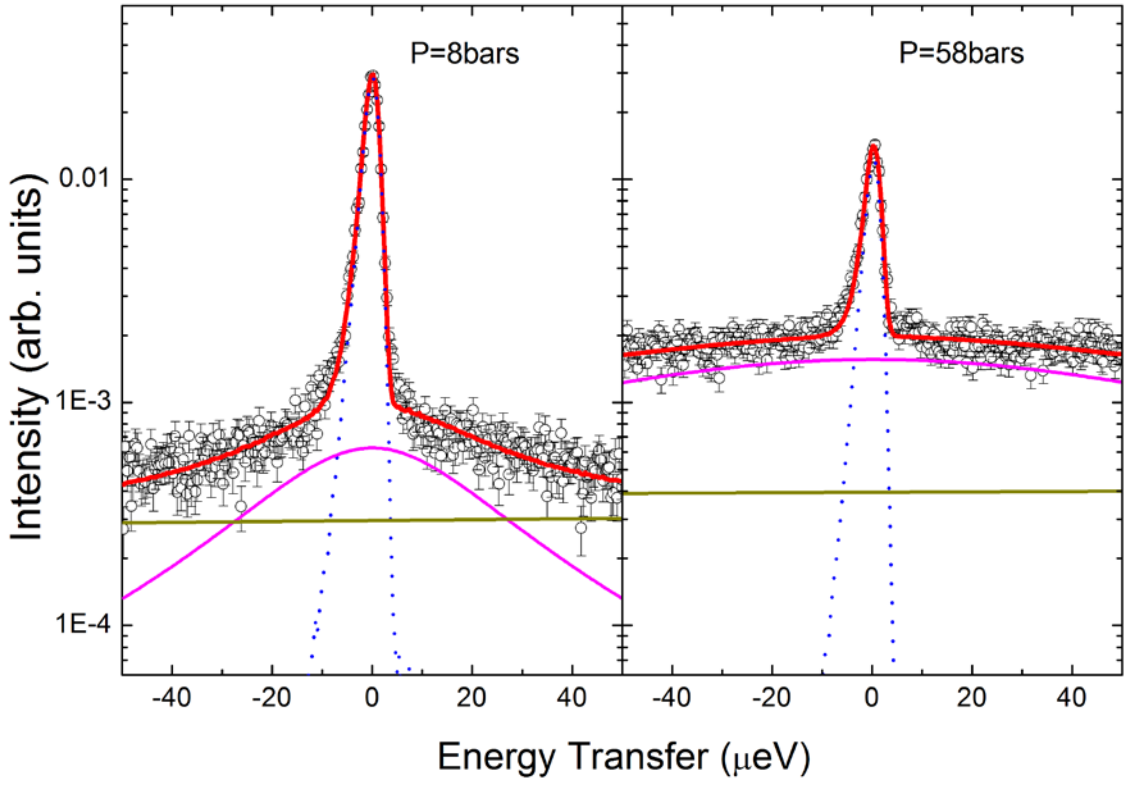

Figure 3. Representative experimental QENS spectra collected at 337 K for propane in silica aerogel and fits with Equation 4 at different pressures and at Q=0.9 Å^{-1}.[23] Experimental data are represented with open circle symbols while the total fit and fit components are represented by lines. Solid red line represents the total fit while the solid magenta and green lines represent the quasielastic component with Lorentzian profile and background contributions respectively. The elastic component is shown with a blue dotted line.

One can see that Eq. 2 with $f(Q,\omega)$ given by Eq. 3 can be obtained by taking a Fourier transform of the equation

$$I(Q,t) = A(Q) + B(Q)e^{-t/\tau(Q)} \qquad (5)$$

In Eq. (5), τ is related to $\Gamma(Q)$ by the relation

$$\Gamma(Q) = \frac{\hbar}{\tau(Q)} \qquad (6)$$

The quantity $I(Q,t)$ is the self-intermediate scattering function corresponding to hydrogen atoms and is the inverse Fourier transform of $S_{inc}(Q,\omega)$. $B(Q)$ is a time independent prefactor of the exponential. Thus, *EISF* ($A(Q)$) can also be seen as the time independent value of $I(Q,t)$ at long times. The quantity $I(Q,t)$ can be calculated directly from the MD simulations as

$$I(Q,t) = \langle \exp(i\boldsymbol{Q}.[\boldsymbol{r}(t+t_0) - \boldsymbol{r}(t_0)]) \rangle \qquad (7)$$

In Eq. (7) $\boldsymbol{r}(t + t_0)$ and $\boldsymbol{r}(t_0)$ are the positions of a given entity in the simulation at times $t + t_0$ and t_0 respectively and $i=\sqrt{-1}$. Averages are carried out over all molecules and all time origins t_0 and different $\boldsymbol{Q}$ with the same magnitude. The last averaging is the powder averaging necessary to compare with the experiments on a powder sample with no preferred orientation. Further, this function can be calculated for contributions from translational motion and rotational motions by separating the co-ordinates of an interaction site (for example CH_3) ($\boldsymbol{r}$) into co-ordinates of the center of mass (COM) of the molecules ($\boldsymbol{r}_{COM}$) and co-ordinates of that site in the center of mass frame ($\boldsymbol{d}$). Thus

$$\boldsymbol{r} = \boldsymbol{r}_{COM} + \boldsymbol{d} \qquad (8)$$

Purely translational motion of the molecules can be studied by following the evolution of $\boldsymbol{r}_{COM}$ in time, whereas rotational motion can be studied by following the evolution of a unit vector ($\boldsymbol{e}$) along $\boldsymbol{d}$ in time. Self-intermediate scattering functions for the two motions can be calculated by replacing $\boldsymbol{r}$ in Eq. 7 by $\boldsymbol{r}_{\mathrm{COM}}$ to obtain the translational intermediate scattering function (TISF) and by $\boldsymbol{e}$ to obtain rotational intermediate scattering function (RISF).

Some representative TISF for 3 different Q values are shown in Figure 4. These curves are extracted from the simulated MD trajectories of propane in the slit pore of Figure 1. Three regimes can be identified from the results shown in Figure 4. Initially the TISFs decay at a fast rate up to a few picoseconds. This is the short-time range corresponding to very fast motion inaccessible to the backscattering instrument, BASIS used in the QENS experiment. A second regime can be identified at the time scales from a few picoseconds to a few tens of picoseconds. This is the intermediate time regime with time scales accessible to the QENS instrument employed in Ref. 23. After a few tens of picoseconds, the TISF data are very noisy. However, in

spite of this noise a very slow decay of the TISF can be seen that indicates very slow motions accessible only to a neutron spin echo instrument with a high resolving power. It can be seen that in the sub-picosecond time range, the TISFs obtained from the lower pressure MD simulation data decay faster than those obtained from simulations at higher pressure, indicating that the corresponding molecular motion is faster at low pressures. In the intermediate time range, which is accessible to the QENS instrument of Ref. 23, one can see that the TISF calculated from the MD simulations decay faster at higher pressure than at low pressure. This observation suggests faster motion at high pressure, in agreement with the experimental findings. Moreover, we can also observe that the simulated TISFs do not decay completely within the intermediate time range (range accessible to the instrument used in Ref 23) indicating that the corresponding experimental spectra could be expected to have a finite elastic component with non-zero EISF values. In this time range, TISF values for the low-pressure data are higher than the high-pressure ones. This would imply a higher EISF at low pressures. This was indeed found to be the case in QENS data analysis. However, the EISF values obtained in the experiments cannot be compared quantitatively here as the EISF obtained in the experiment was only relative. The absolute values were not extracted as no background subtraction was carried out[23].

The qualitative information obtained from the behavior of the TISF curves obtained from the simulations can be quantified by modeling the behavior of TISF in the time range accessible to the experiments. As stated above, the experimental data were fitted with Eq. 4, so, ignoring the background term[a], one can expect that the corresponding TISF should be describable by Eq. 5. The relevant portion of the TISF (~ 5 to ~ 25 ps) was modeled with an exponential decay function as shown in Figure 5. The decay constants of the exponential decay functions used to model the TISFs at intermediate times were converted to the energy scale using Eq. 6 and were directly compared with $\Gamma(Q)$ obtained from the experiments (see Figure 6). There is a good agreement between experimental and simulation data although the dispersion in the $\Gamma(Q)$ values obtained from the simulation exhibits a less systematic trend as compared to the experimental data. A major contribution of this noise can be traced to the difficulty in modeling a small quantity. It can be seen that the TISF have already decayed to a hundredth in the time range accessible to the instrument. This small value of TISF is prone to large relative errors, which then propagate to the $\Gamma(Q)$ values obtained from fitting. However, the variation of $\Gamma(Q)$ with pressure is unambiguous and it is in semi-quantitative agreement with the experimental data.

Having thus validated our simulation data by a direct comparison with the experiments, we discuss below other quantities calculated from the simulations.

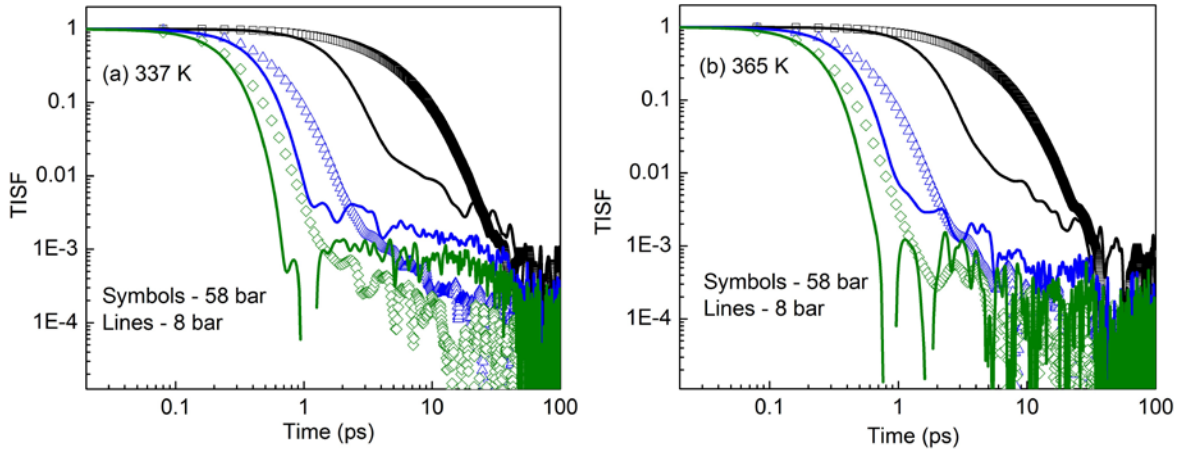

Figure 4. TISFs at (a) 337 K and (b) 365 K, 8 and 58 bar (lines and symbols respectively) at three Q values – 0.3 (black), 1.2 (blue) and 1.8 Å^{-1} (olive). It can be seen that the behavior of TISFs at sub picosecond time scale is different from the long time behavior.

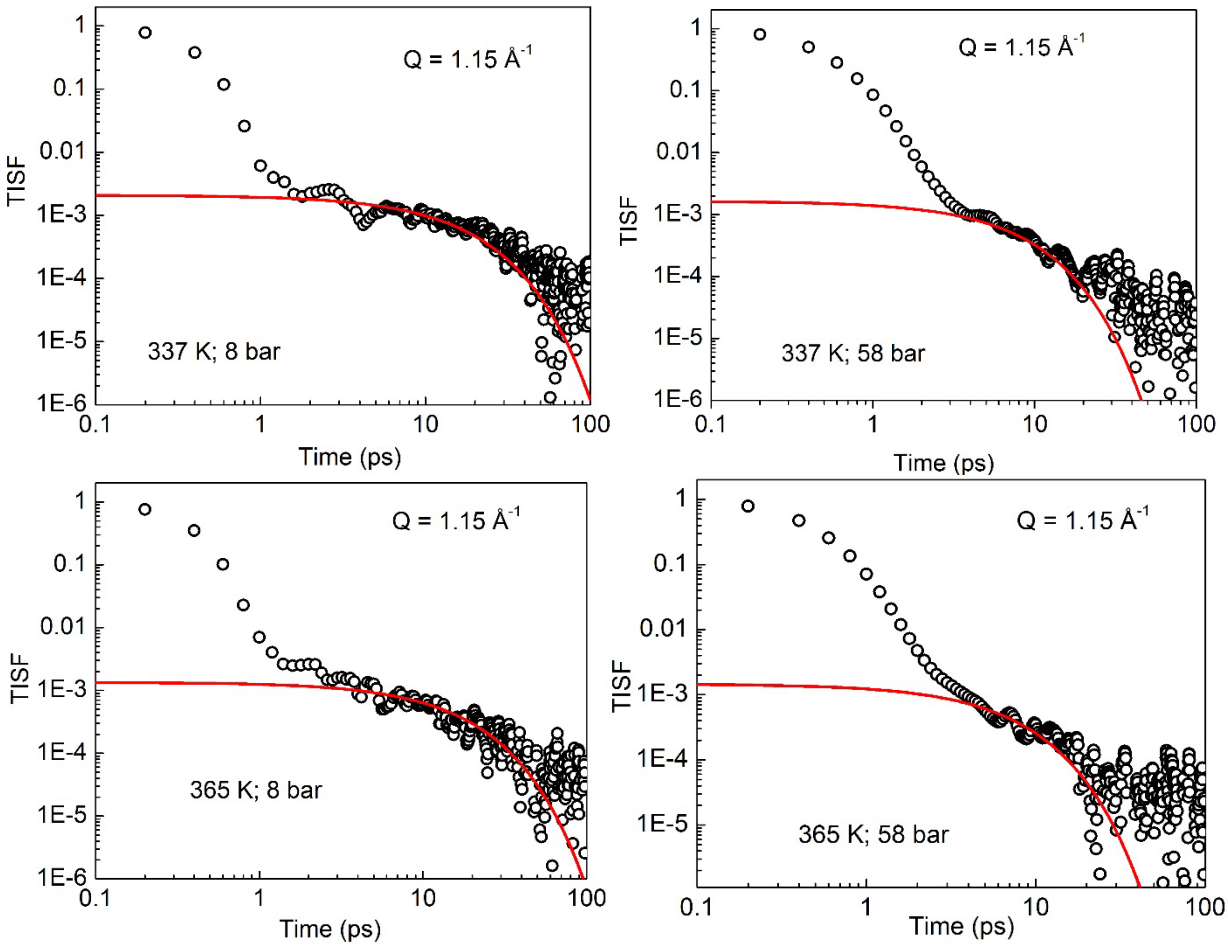

Figure 5. Fits of the intermediate time range of TISF at Q = 1.15 Å^{-1} with exponential decay function (red lines).

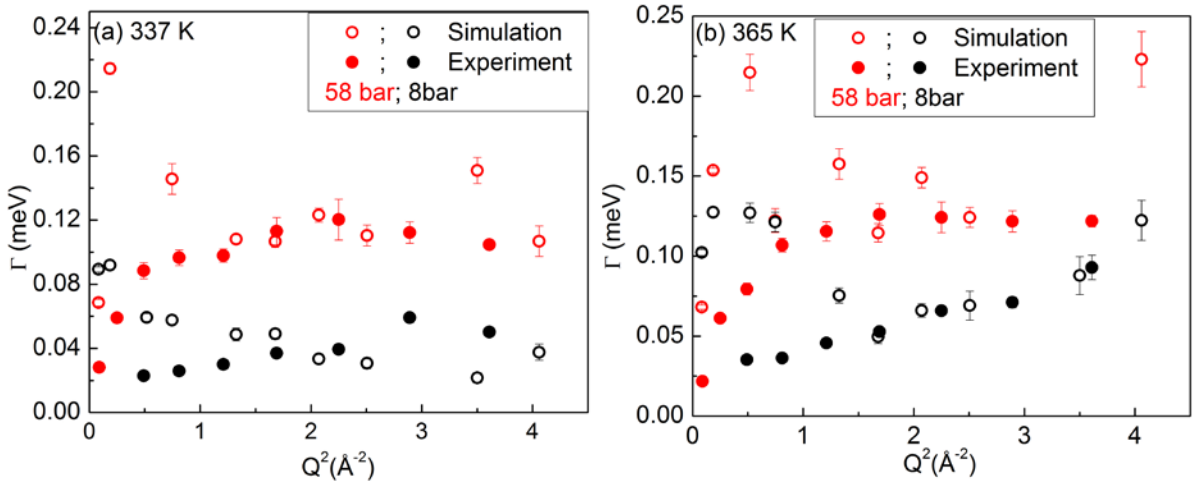

Figure 6. Comparison of the $\Gamma(Q)$ values obtained using Eq. 6 from fits of the TISF from the simulation with exponential decay functions (open symbols) against the $\Gamma(Q)$ values (solid symbols) obtained from fitting of the experimental spectra[23]. Red symbols denote results obtained at 58 bar while the black symbols are for the data at 8 bar. Panel (a) for 337 K and the panel (b) for 365 K.

4. Structure

To probe a possible relation between structural and dynamical properties of propane in the SiO_2 mesopore, we calculated the fraction of total molecules found within a bin of 0.01 nm in the z direction, as a function of their position in the pore. This is shown in Figure 7. A larger fraction of propane molecules lies close to the walls at lower pressure. Further, as can be seen in the inset of Figure 7, there is an indication of formation of a second layer of molecules close to the pore wall. Motion of the propane molecules that are close to the walls is expected to be slow due to relatively strong interactions with the wall, and therefore will contribute little to the overall diffusivity of confined propane. At higher pressure (greater loading), the fraction of molecules close to the wall is comparatively small relative to the entire pore, and consequently the number of more mobile molecules is larger. This change in the fraction of molecules adsorbed near the pore surface vs. those in the pore center enhances the diffusivity at high pressure. The variation in this distribution (adsorbed near the walls vs. near the pore center) at the two temperatures sampled is smaller than that observed when the pressure is varied. Moreover, this variation in temperature gets further diminished at higher pressure. At low pressures, the extra kinetic energy provided to the system in the form of a raised temperature helps some adsorbed molecules

overcome the attractive interactions due to the surface and move away from the pore wall. This phenomenon results in a decrease in the fraction of molecules residing close to the pore wall as the temperature increases. At higher pressure the temperature effect is smaller due to a large total number of molecules. The distribution of propane molecules along the direction of confinement across the pore facilitates classification into interfacial and non-interfacial molecules. In what follows we shall refer to the propane molecules that lie within a distance of 0.3 nm from the pore surface, on both sides, as interfacial molecules and the rest as non-interfacial molecules.

The distribution of interfacial molecules in the XY plane shows some positional ordering, but only at high pressure (Figure S1 in supplementary material). This ordering originates from the crystalline positional ordering of the atoms within the solid SiO_2 matrix. We also calculated the orientational ordering by calculating the cosine of the angle made by the CH_3-COM vector with the Z-direction (Figure S2 in supplementary material). Here again, an ordering is relatively more clearly seen at higher pressure. It is expected that on an amorphous surface the ordering of the adsorbed propane molecules will be less pronounced. However, the enhanced density of propane at the solid-fluid interface is expected both on crystalline and amorphous substrates.

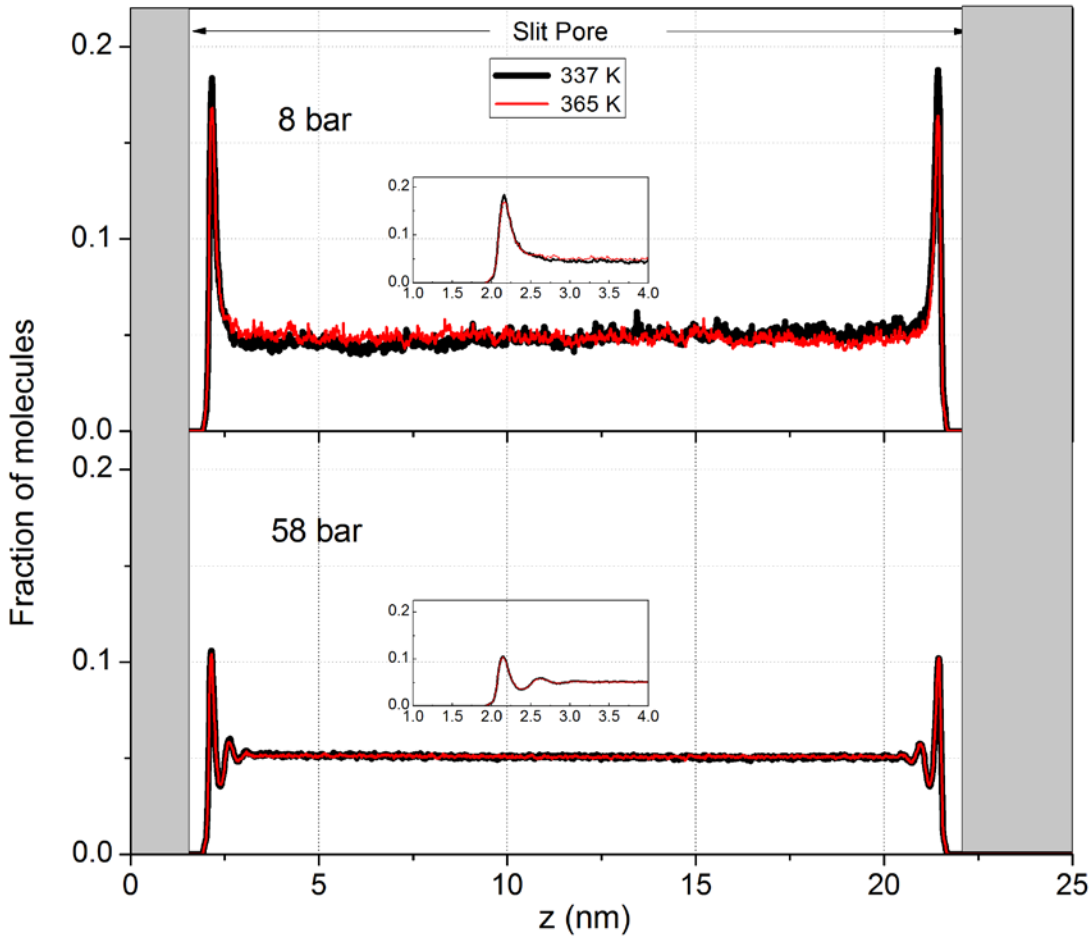

Figure 7. Fraction of total number of molecules occupying the pore as a function of the position within the direction perpendicular to the pore surfaces for 8 bar (top) and 58 bar (bottom). The pore space is between the two grey regions. The region between z=1.0 to 4.0 nm is shown in the inset to highlight the difference in the layering at two pressures.

To quantify whether an overall preferred orientation of propane molecules exists throughout the pore we calculated the orientational distribution of interfacial and non-interfacial propane molecules. Figure 8 shows the distribution of the orientation of a CH_3 site in the molecular frame of reference with respect to the three Cartesian directions. For reference the distribution function expected when there is no orientational ordering (i. e. isotropic distribution) is also shown with a thick cyan line. It can be seen that in the center of the pore the distribution is isotropic whereas there seems to be a tendency towards orientational ordering among interfacial molecules. This is revealed by the distribution with respect to Z-direction, which becomes sharper at right angle and those with respect to the X and Y-directions that get suppressed at right angle. This means that

interfacial propane molecules have a slight weak preference to orient in such a way that the CH_3-CH_2 bond is aligned parallel to the pore surface. To quantify this preference we define an anisotropy parameter as a measure of deviation from isotropic behavior as

$$\varphi = \sqrt{\frac{1}{N}\sum_i^N \left(g_{iso}(\theta_i) - g_{prop}(\theta_i)\right)^2} \qquad (9)$$

where g is the orientational distribution function and the subscripts *iso* and *prop* stand for the isotropic case and the observed case of propane in silica slit pore, respectively. The sum is taken over N=3151 different values of the angle θ_i between 0 and 180° for which the distribution functions were calculated. Values of this anisotropy parameter with respect to the three Cartesian directions, for interfacial and non-interfacial molecules are listed in Table 1. A higher value of φ signifies a stronger preference for a particular orientation. In general, anisotropy is higher at lower pressure and for interfacial molecules. This is to be expected as the interfacial molecules interact closely with the pore surface and hence follow the ordered structure of the pore surface thereby showing a stronger tendency for orientational ordering. At higher pressure, the number of molecules is larger than that can be accommodated with the orientational ordering and the excess molecules occupy random orientations thereby decreasing the relative anisotropy. A similar decrease in anisotropy at higher loadings has been found in ethane confined in ZSM-5 zeolite[49]. This behavior has consequences for the rotational motion of propane molecules at different pressures. Note that the anisotropy of the orientation of interfacial molecules is due to both the atomic arrangement of the substrate and the packing of the propane molecules at the interface, which would occur also on an amorphous substrate.

Table 1. Anisotropy parameter φ ($\times 10^{-6}$) as defined in Eq. 9 for propane molecules at 337 K.

Pressure	Interfacial molecules			Non-interfacial molecules		
	X	Y	Z	X	Y	Z
8	23.36	21.35	32.11	7.76	7.74	7.97
58	8.02	3.52	13.40	1.75	1.75	1.79

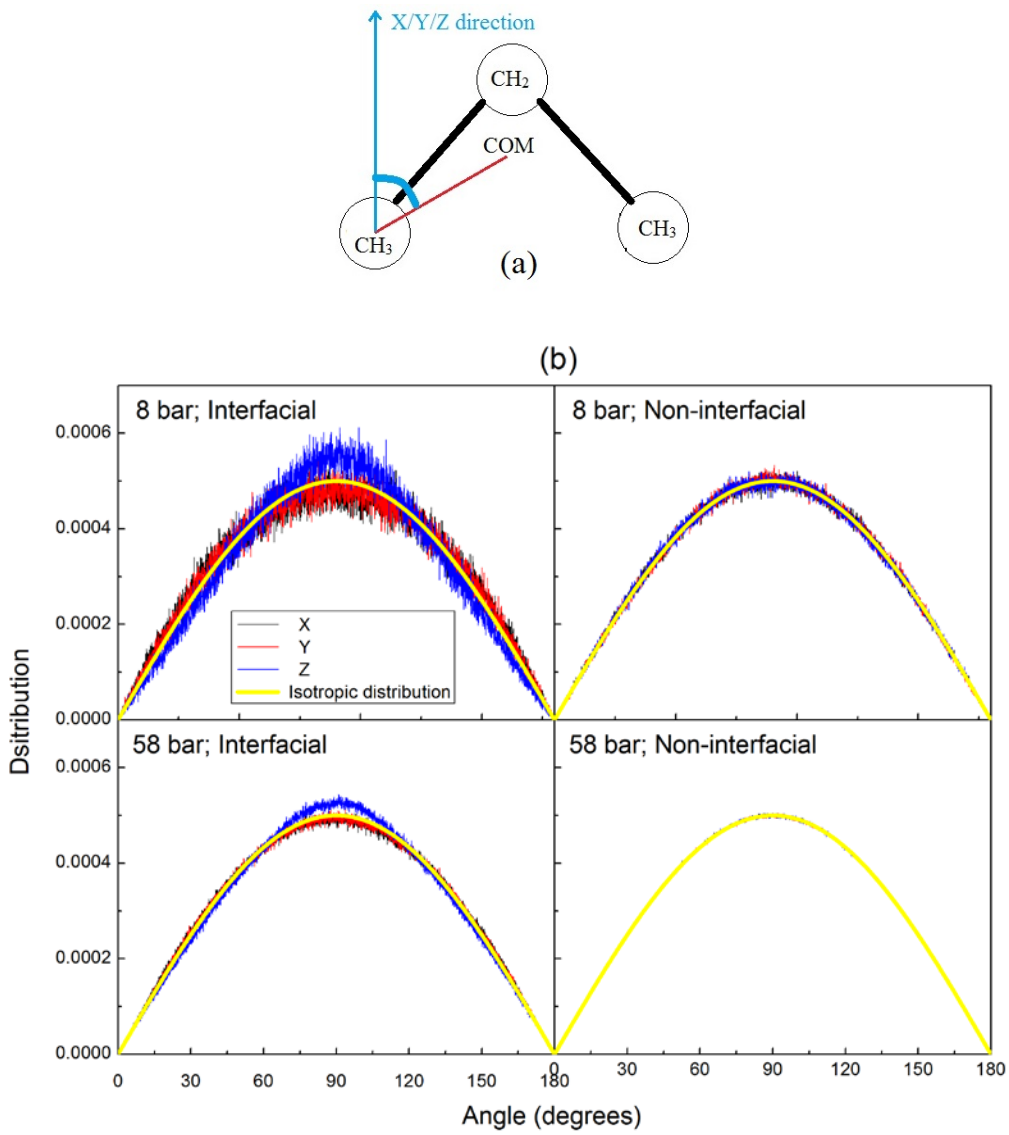

Figure 8. (a) Schematic showing the angle made by the CH_3 position vector in the molecular (COM) frame of reference with the Cartesian directions denoted by a cyan line. (b) Orientational distribution of the angle defined in (a) with respect to the Cartesian directions X (black), Y (red) and Z (blue) at 337 K and 8 bar (top) and 58 bar (bottom). Left panels show the distribution for interfacial molecules whereas the right panels show the distribution for non-interfacial molecules. For reference the expected curve for an ideal isotropic distribution is shown as a thick yellow line in all panels.

5. Dynamics

1. Translational motion

Information about the overall translational motion can be obtained by studying the evolution of mean squared displacement (MSD) with time. We calculated MSD using the COM trajectories of the propane molecules as

$$MSD = \langle |\boldsymbol{r_{COM}}(t + t_o) - \boldsymbol{r_{COM}}(t_0)|^2 \rangle \qquad (10)$$

In Eq. (10) the ensemble average is taken over all molecules and time origins t_0. Figure 9 shows the MSD variation for the four conditions of temperature and pressure. The MSD at lower pressure is an order of magnitude higher than that at high pressure. The variation with temperature is less pronounced than that observed due to pressure changes, and it becomes weaker at high pressure. This could be an effect of a crowded environment at higher pressure. Another interesting feature that can be observed is the change in behavior of MSD with time. The initial short time ballistic motion, where a molecule moves free of collisions, extends up to about 30 ps at lower pressures while it lasts less than 1 ps at higher pressure. This is also a consequence of molecular crowding, as a higher number of neighboring molecules at high pressure makes intermolecular collisions more frequent. At the time when ballistic motion turns diffusive (marked with arrows in Figure 9, a typical molecule would have covered a distance equal to the mean free path. Assessing the MSD values at times where ballistic motion turns diffusive, the mean free path can be estimated to be ~ 10 nm at low pressures and about 0.3 nm at high pressure. Thus at high pressure, propane seems to behave as a viscous fluid while at low pressure it is close to transition between a viscous fluid and a Knudsen fluid.[50]

Self-diffusion coefficients (D_s) are obtained, from the slope of the MSD versus time at long enough times where the motion is diffusive, using the relation

$$D_s = \lim_{t\to\infty} \frac{MSD}{2n_d t} \qquad (11)$$

where n_d=3 is the number of degrees of freedom. Our results are enlisted in Table 2. The diffusion coefficients obtained from MSD plots are 3 orders of magnitude faster than those obtained from the QENS experiments[23]. This might be due to the geometry of the pores used in our simulations, which is an over-simplification compared to the aerogels used in the experiments, and could also be due to the limitations of the force fields implemented. These diffusion coefficients are however comparable to the planar diffusion coefficient of propane in a silica slit pore of 2.8 nm obtained earlier[36]. The large order of magnitude difference between the experiments and the present simulations can also be explained as a consequence of the limitations of the experiment. In QENS, the diffusion coefficient is obtained from fitting the dispersion in quasielastic widths ($\Gamma(Q)$) obtained from the experiment with a model. Each QENS

instrument has a limited energy transfer window and a finite resolution, which results in detection of only those molecules that exhibit energies over a finite range. The contribution from faster molecules to the QENS spectra would lead to a very broad feature that appears as a flat background. This contribution would therefore not be included in the $\Gamma(Q)$ obtained from fitting the spectra with a Lorentzian profile. In the case of a very large pore, some molecules, especially at low pressures would move faster than the detectable energy range and be invisible to the QENS instrument even though they do contribute to the mean squared displacement in the simulation. Another limitation stems from the Q dependence of the experimental data. As $\boldsymbol{Q}$ is a vector in reciprocal space, its magnitude has dimensions of $(\text{length})^{-1}$ and thus encodes information on length scales. The Q dependence of TISFs in the simulation and scattering law in the experiment limits detection of motion within a finite range of length scales, whereas MSD being a function of only time captures motion at all length scales.

Table 2. Self-diffusion Coefficients obtained from the variation of MSD with time.

Temperature (K)	Pressure (bar)	Self-diffusion Coefficient ($\times 10^{-10}$ m^2/s)
337	8	5738.36±0.31
	58	331.22±0.09
365	8	6333.03±0.92
	58	332.20±0.16

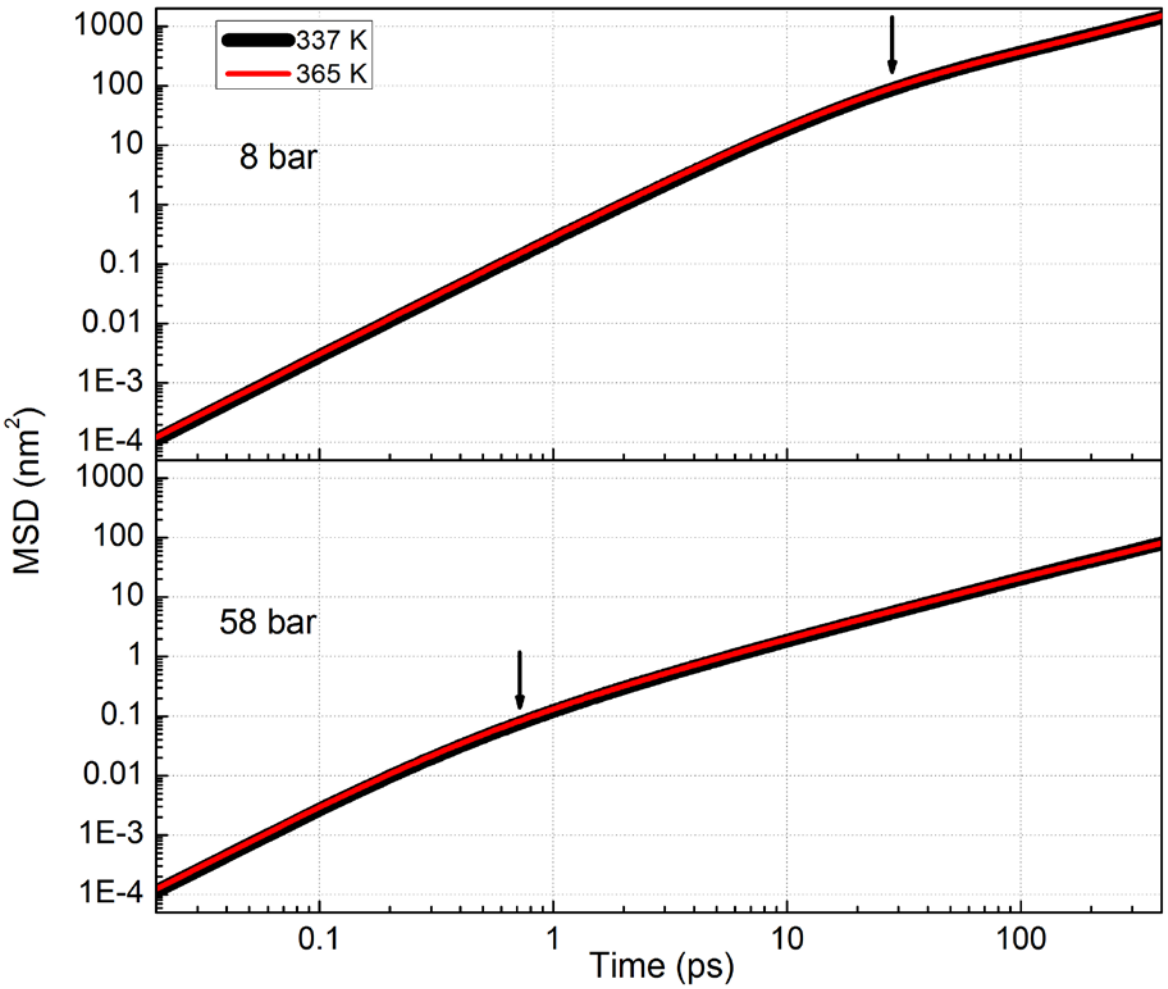

Figure 9. Mean squared displacement (MSD) curves for propane in silica slit pore at 337 K (black) and 365 K (red) at the two pressures, 8 bar (top) and 58 bar (bottom). Transition from ballistic to diffusive regimes is indicated by arrows.

To study the effect of interaction with the pore walls we obtained the trajectories of 10 molecules that spent 50 ps at a time in the interfacial and non-interfacial regions (see Figure S3, Supplementary material) for the two simulations at 337 K. Several properties were calculated from these short trajectories including MSD (see Figure S4).

2. Rotational Motion

The rotational molecular motion of propane was probed by following the evolution of a unit vector (***e***) attached to the position vector of a CH_3 site in the molecular frame of reference. In particular we calculated the orientational correlation functions (OCF) of order 1 and 2.

$$C_l(t) = \langle P_l[\boldsymbol{e}(t + t_0).\boldsymbol{e}(t_0)]\rangle \qquad (12)$$

where $C_l(t)$ is the OCF of order l and $P_l(x)$ is the Legendre's polynomial of order l. The first of these functions (l=1) is the dipole correlation function and is often used to study rotational motion[51-53]. The second order component (l=2) is related to the Fourier transform of spectral density measurable in NMR experiments. Figure 10 shows the OCF for the four MD simulations. As in the case of translational motion, the variation of OCF as a function of pressure is dominant over the effect of temperature. The first order OCF at low pressures shows a conspicuous negative dip. This is a signature of a rotational motion characterized by large angular jumps. The time scales of rotational motion can be obtained by integrating the OCF up to times long enough for these functions to decay to zero[51]. We integrated the OCF up to 40 ps to obtain the time scales from OCF of order 1 and 2. They are listed below in Table 3. The rotational motion gets faster at higher pressures. A similar enhancement of rotational motion with increase in loading has been observed for ethane in ZSM-5 both in simulations[49] as well as in experiments[54], as also for propane in TiO_2[51]. Further, in Ref. 49, this enhancement of rotational motion was explained on the basis of a reduced anisotropy at higher loadings. The pressure dependence of rotational motion in the present case of propane in silica pore bears the same correlation with the pressure dependence of anisotropy as can be seen from Tables 1 and 3. Also listed in Table 3 are the ratios of the two time scales of rotational motion. The Debye model of rotational model predicts a value of 3.0 for this ratio[55]. Our results differ significantly from this expectation. The deviation is further enhanced at low pressures. These time scales have the same order of magnitude as obtained for propane in 4 nm cylindrical pores of TiO_2[51]. We note that these time scales indicate a very fast rotation which convert to an energy scale of ~ 1 meV (see Eq. 6). This means that the quasielastic broadening from the rotational motion of propane molecules in 20 nm silica pores would be too strong to be seen with the BASIS instrument with an energy window of ±0.12 meV, used in Ref. 23. This justifies the assumption made in the analysis of QENS data that the signal represented only the translational motion of propane molecules.

Table 3. Time scales of rotational motion.

T; P	τ_1(ps)	τ_2(ps)	τ_1/τ_2
337 K; 8 bar	0.631	0.818	0.7714
365 K; 8 bar	0.635	0.813	0.7811

337 K; 58 bar	0.355	0.203	1.749
365 K; 58 bar	0.33	0.19	1.737

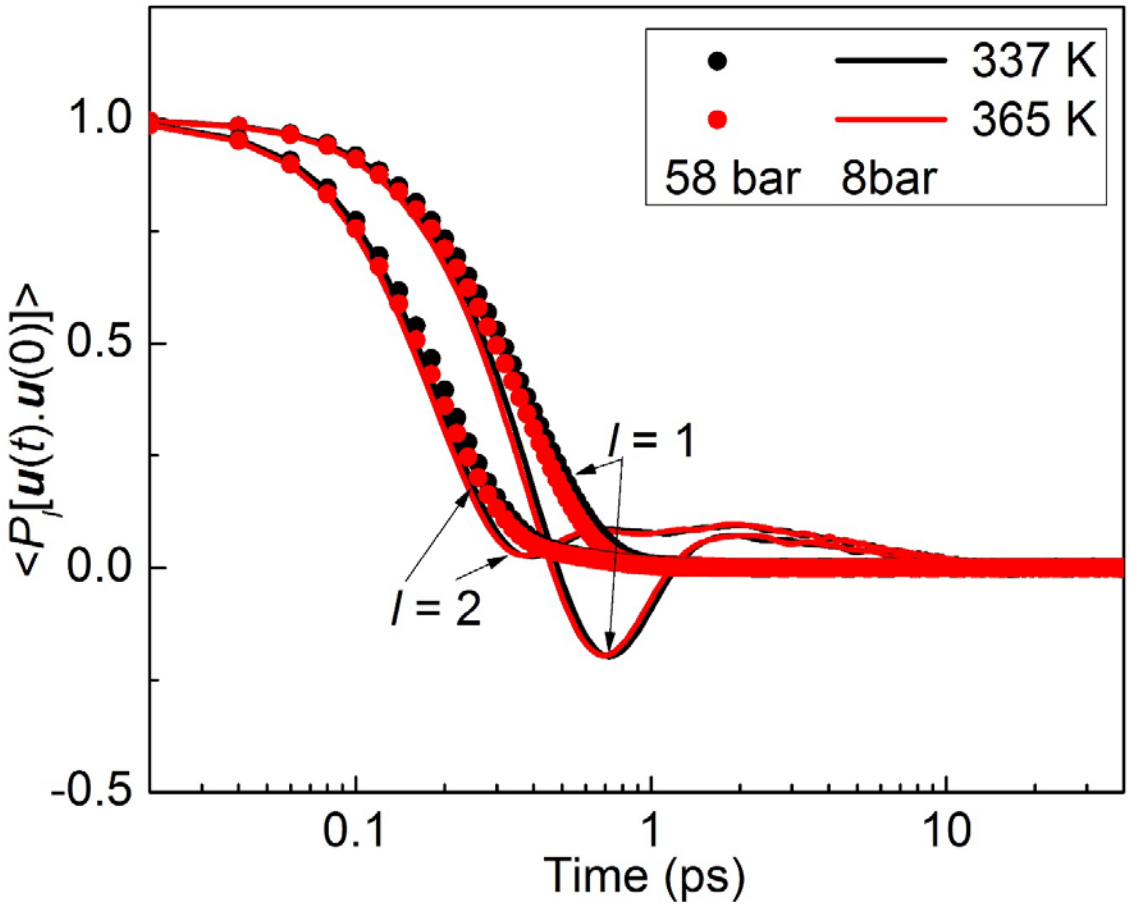

Figure 10. Orientational Correlation Functions (OCF) for different temperatures and pressures.

The orientational dynamics of interfacial and non-interfacial propane molecules was probed using the OCF corresponding to the 10 representative molecules from the two populations separately (Supplementary material, Figure S5). Compared to the OCF of non-interfacial molecules, those of interfacial molecules were found to decay slowly indicating a slower rotation of interfacial molecules as is expected due to the strong fluid-surface interactions.

In addition to the OCF, the rotational intermediate scattering functions (RISF) for propane in silica pore were also calculated. These functions for 6 different *Q* values at two temperatures and two pressures are shown in Figure 11. The overall qualitative information content in these functions is similar to that in the OCF. However, these functions provide additional information

on the geometry of rotational motion by their long time behavior, which is identical to the elastic incoherent structure factor EISF. The variation of EISF in *Q* can reveal the geometry of motion. It should be noted that the EISF obtained from simulated RISF only represents the rotational motion, and are thus different from the EISF values obtained in the experiment, which can have contribution from rotational as well as localized translational motion. For clarity, we use REISF to signify the EISF obtained from the simulated RISF. Results in Figure 11 indicate that the differences in RISFs for different temperatures and pressures are limited to very short times up to 20 ps. After this time, the RISF for a given *Q* value for different *T* and *P* conditions converge implying that the REISF values and hence the geometry of rotational motion remains unchanged between different *T* and *P* conditions. The variation of REISF obtained is shown in Figure 12. Also shown in Figure 12 is the calculated REISF for a unit vector undergoing isotropic rotational diffusion. The match between the calculated REISF for this model and the REISF values obtained from the simulation is very good. This is to be expected as the propane molecules near the pore center exhibit little preference for a particular orientation and would therefore freely span the whole orientational space corresponding to isotropic rotation.

The RISF were also calculated for the interfacial and non-interfacial molecules separately (see Figure S6 in supplementary material). No change in the REISF values was observed as the pressure or the location of propane molecules is changed. This means that the geometry of rotational motion remains unchanged for all the simulation conditions, for all molecules. This can be expected as very little orientational ordering is observed from the orientational distribution function for all simulations. The only change that comes about the rotational motion is thus a change in the speed of rotation and the extent of angular jumps.

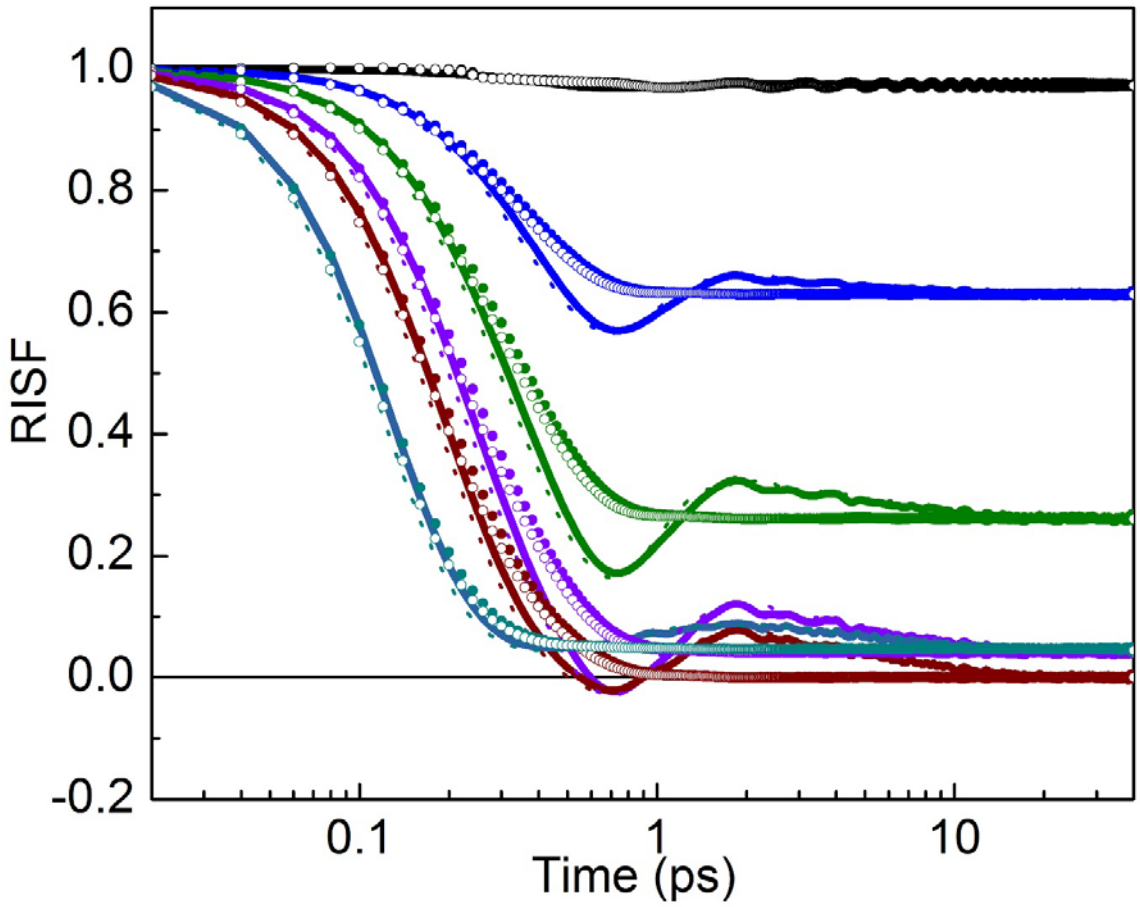

509

510 **Figure 11**. Rotational Intermediate Scattering Functions (RISFs) for different temperatures and pressures
511 for *Q* values between 0.29 and 4.6 $Å^{-1}$ (top to bottom at 0.1 ps). Low pressure data is represented by lines
512 whereas symbols are used to show the high pressure data. Thick lines and solid symbols represent 337 K
513 data while the 365 K data is shown by thin lines and open symbols.

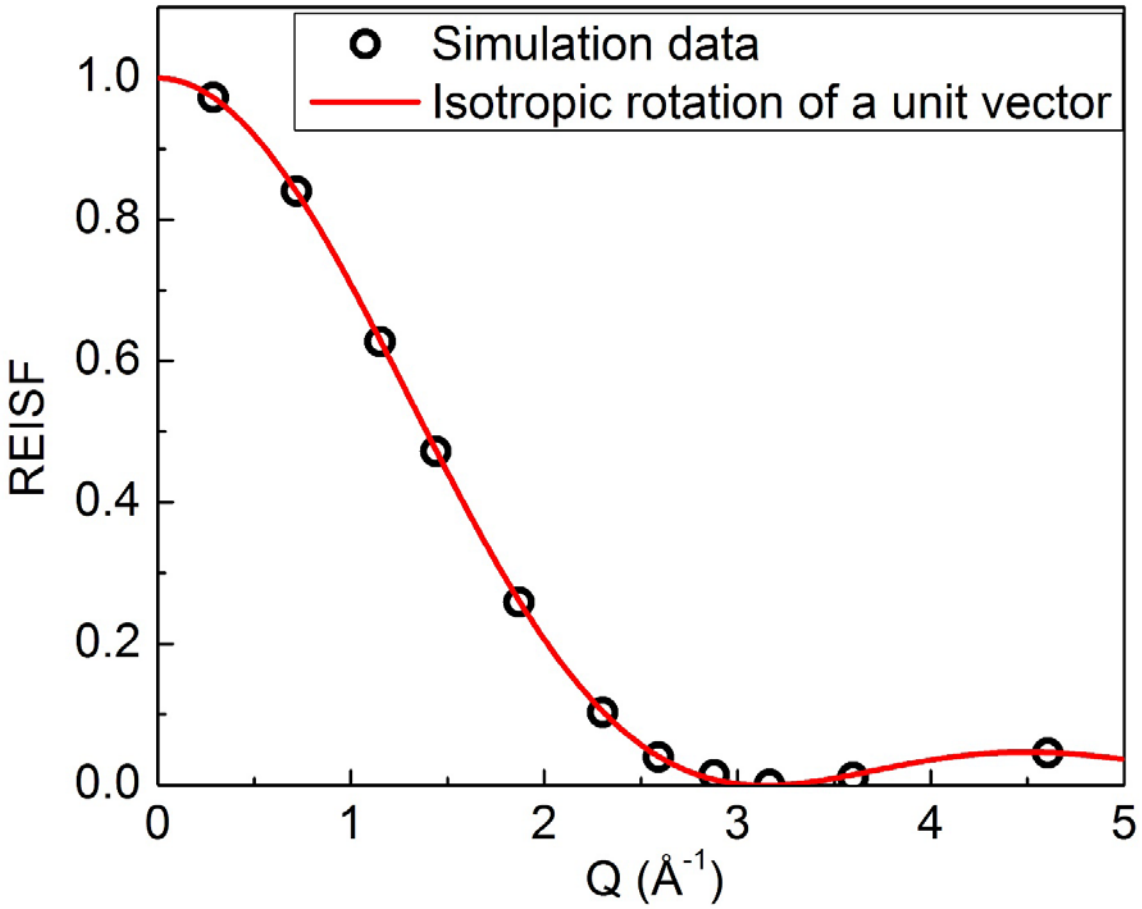

Figure 12. REISF obtained from the long time values of RISFs from the simulation (symbols). Solid red line is the calculated REISF variation for a unit vector undergoing isotropic rotational diffusion.

6. Conclusions

We reported a direct comparison of molecular dynamics (MD) simulations of propane in 20 nm slit pore of silica with QENS experiments carried out on propane in silica aerogel with ~20 nm pores. Time scales obtained from the intermediate scattering functions from these simulations agree well with the experimental data. Although the simulated mean square displacement curves do not seem to agree with the experimental finding of an enhanced diffusion at higher pressures, the latter is corroborated with the time scales obtained from TISFs. It is important to note that while MSD curves give a length scale averaged contribution to diffusivity, the TISFs take into account motion at different length scales by the virtue of their Q dependence. This difference in MSD and TISFs might help explain the discrepancy observed in the pressure dependence of time scales obtained from these quantities. A larger fraction of propane molecules residing close to

the pore wall at low pressure explains the enhancement of diffusivity at high pressure observed in the QENS experiments[23]. Overall, the rotational motion of propane molecules is isotropic at all temperatures and pressures, and in all the regions of the pore. The time scales obtained from the simulation suggest that the rotational motion of propane molecules in the pore is too fast to be captured by the QENS instrument used in the experiment reported in Ref. 23 and thus justifies modeling the QENS spectra with translational motion alone. Rotational motion also shows a slight enhancement at higher loading similar to findings elsewhere[49,51,54]. This is correlated with a higher degree of orientational anisotropy at lower loading which provides an explanation to this anomalous behavior. Although the simulated system is an oversimplification of the experimental one, our analysis suggests that MD simulations reported here reveal important new insight about anomalous loading dependence of propane dynamics in silica mesopores.

CONFLICT OF INTEREST

There is no conflict of interest to declare.

ACKNOWLEDGEMENTS

We acknowledge the financial support from the U.S. Department of Energy, Office of Basic Energy Sciences, under Contract No. DE-SC0006901 (Division of Chemical Sciences, Geosciences, and Biosciences). AS acknowledges financial support from the European Union via a Marie Curie Career Integration Grant. Generous allocations of computing time were provided by the University College London Research Computing Platforms Support (LEGION) and the Sloan Foundation-funded Deep Carbon Observatory cluster hosted by Rensselaer Polytechnic Institute (Peter Fox and Patrick West).

Notes

[a] The background term in the experiment would signify contributions from several sources including the silica aerogel. The TISF calculated from the simulated trajectories on the other hand has contribution from the center of mass motion of propane molecules alone and so would

not have any contribution analogous to the background contribution in the experiment. The background term should therefore be ignored.

References

[1] Cole, D. R., Herwig, K., Mamontov and E., Larese, L., in Wenk, H-R (Ed.) Neutron Scattering in Earth Sciences, *Rev Min. Geoc*. **2006**, *63*, 313-362.

[2] Cole, D. R., Mamontov, E. and Rother, G. in Liang, L., Rinaldi, R. and Schoeber, H., (Eds.) Neutron Applications in Earth, Energy, and Environmental Sciences, **2009**, 547-570.

[3] Cole, D. R., Grszkiewicz, M. S., Simonson, J. M., Chialvo, A. A., Melnichenko, Y. B., Wignall, G. D., Lynn, G. W., Lin, J. S., Habenschuss, A., Gu, B., et al., "Influence of Nanoscale Porosity on Fluid Behavior" In: Water-Rock Interaction, 737-740, (Wanty, R. B. and Seal II, R. R. Eds.) Taylor & Francis, London **2004.**

[4] Karger, J. Long-time Limit of the Self-Correlation-Function of One-Dimensional Diffusion, *Phys. Rev. E*, **1993**, *47*, 1427-1428.

[5] Hahn, K., Karger, J. and Kukla, V. Single-File Diffusion Observation, *Phys. Rev. Lett*., **1996**, *76*, 2762-2765.

[6] Bhide, S. Y. and Yashonath, S. Dependence of the Self-Diffusion Coefficient on the Sorbate Concentration: A Two-Dimensional Lattice Gas Model With and Without Confinement, *J. Chem. Phys.*, **1999**, *111*, 1658-1667.

[7] Bhide, S. Y. and Yashonath, S. Types of Dependence of Self-Diffusivity on Sorbate Concentration in Parameter Space: A Two-Dimensional Lattice Gas Study, *J. Phys. Chem. B,* **2000**, *104*, 2607-2612.

[8] Ghorai, P. K., Yashonath, S., Demontis, P. and Suffritti, G. B. Diffusion Anomaly as a Function of Molecular Length of Linear Molecules: Levitation Effect, *J. Am. Chem. Soc.*, **2003**, *125*, 7116-7123.

582 [9] Wasyluk, L., Peplinska, B., Klinowski, J. and Jurga, S. NMR Studies of the Molecular
583 Dynamics of Tert-Butyl Chloride Confined in the Mesoporous Molecular Sieve MCM-41, *Phys.*
584 *Chem. Chem. Phys.*, **2002**, *4*, 2392-2397.

585 [10] Melnichenko, Y. B., Schuller, J., Richert, R., Ewen B. and Loong, C.K. Dynamics of
586 Hydrogen-Bonded Liquids Confined to Mesopores: A Dielectric and Neutron Spectroscopy
587 Study, *J. Chem. Phys.*, **1995**, *103*, 2016-2024.

588 [11] Bergman, R. and Swenson, J. Dynamics of Supercooled Water in Confined Geometry,
589 *Nature*, **2000**, *403*, 283-286.

590 [12] Liu, L. Chen, S.-H., Faraone, A., Yen, C.-W., Mou, C.-Y., Kolesnikov, A.I., Mamontov, E.
591 and Leao, J. Quasielastic and Inelastic Neutron Scattering Investigation of Fragile-to-Strong
592 Crossover in Deeply Supercooled Water Confined in Nanoporous Silica Matrices, *J. Phys. Cond.*
593 *Mat.*, **2006**, *18*, S2261-S2284.

594 [13] Gautam, S., Mitra, S. and Mukhopadhyay, R. Molecular Motion in Restricted Geometries,
595 *Pramana- J. Phys.*, **2008**, *71*, 809-818.

596 [14] Adrjanowicz, K., Kolodziejczyk, K., Kipnusu, W. K., Tarnacka, M., Mapesa, E. U.,
597 Kaminska, E., Pawlus, S., Kaminski, K., Paluch, M. Decoupling between the Interfacial and
598 Core Molecular Dynamics of Salol in 2D Confinement. *J. Phys. Chem. C*. **2015,** *119*, 14366 –
599 14374.

600 [15] Camisasca, G., De Marzio, M., Rovere, M., Gallo, P. Slow Dynamics and Structure of
601 Supercooled Water in Confinement. *Entropy*. **2017**, *19*, 185.

602 [16] Mandal, S., Spanner-Denzer, M., Leitmann, S., Franosch, T. Complex dynamics induced by
603 strong confinement–From tracer diffusion in strongly heterogeneous media to glassy relaxation
604 of dense fluids in narrow slits. *Eur. Phys. J. Spec. Topics*. **2017,** *226*, 3129-3156.

605 [17] Le, T., Striolo, A., Turner, C. H., Cole, D. R. Confinement Effects on Carbon Dioxide
606 Methanation: A Novel Mechanism for Abiotic Methane Formation. *Sci. Rep.* **2017**, *7*, 9021.

607 [18] Phan, A., Cole, D. R., Weiß, R. G., Dzubiella, J., Striolo A. Confined water determines
608 transport properties of guest molecules in narrow pores. *ACS Nano*. **2016,** *10*, 7646 – 7656.

[19] McNaught, A. D. and Wilkinson, A. IUPAC Compendium of Chemical Terminology, 2nd ed. (the "Gold Book"); Blackwell Scientific Publications: Oxford, U.K., **1997**.

[20] Chialvo A. A. and Vlcek, L. Can We Decribe Graphene Confined Water Structures as Overlapping of Approaching Graphene-Water Interfacial Structures?, *J. Phys. Chem. C* **2016**, *120*, 7553-7561.

[21] Patankar, S., Gautam, S., Rother, G., Podlesnyak, A., Ehlers, G., Liu, T., Cole, D. R., and Tomasko, D. L. Role of Confinement on Adsorption and Dynamics of Ethane and an Ethane-CO_2 Mixture in Mesoporous CPG Silica, *J. Phys. Chem. C* **2016**, *120*, 4843-4853.

[22] Chathoth, S. M., Mamontov, E., Melnichenko, Y. B. and Zamponi, M. Diffusion and Adsorption of Methane Confined in Nano-Porous Carbon Aerogel: A Combined Quasi-Elastic and Small-Angle Neutron Scattering Study, *Micro. Meso. Mater.*, **2010**, *132*, 148-153.

[23] Gautam, S., Liu, T., Rother, G., Jalarvo, N., Mamontov, E., Welch, S., Sheets, J., Droege, M., and Cole, D. R. Dynamics of Propane in Nanoporous Silica Aerogel: A Quasielastic Neutron Scattering Study, *J. Phys. Chem. C*, **2015**, *119*, 18188-18195.

[24] Bee, M. Quasielastic Neutron Scattering, Adam Hilger, Bristol **1988**.

[25] Morelon, N-D., Kneller, G. R., Ferrand, M., Grand, A., Smith, J. C., and Bée, M. Dynamics of alkane chains included in an organic matrix: Molecular dynamics simulation and comparison with neutron scattering experiment, *J. Chem. Phys.* **1998**, *109*, 2883 – 2894.

[26] Jobic, H., and Theodorou, D. N. Quasi-elastic neutron scattering and molecular dynamics simulation as complementary techniques for studying diffusion in zeolites, *Micro. Meso. Mat.* **2007**, 102, 21 – 50.

[27] Mukhopadhyay, R., Sayeed, A., Mitra, S., Kumar, A. V. A., Rao, M. N., Yashonath, S. and Chaplot, S. L. Rotational Dynamics of Propane in Na-Y Zeolite: A Molecular Dynamics and Quasielastic Neutron Scattering Study, *Phys. Rev. E*, **2002**, *66*, 061201

[28] Gautam, S., Mitra, S., Mukhopadhyay, R. and Chaplot, S. L. Diffusion of Acetylene inside Na-Y Zeolite: Molecular Dynamics Simulation Studies, *Phys. Rev. E*, **2006**, *74*, 041202.

635 [29] Gautam, S., Mitra, S., Chaplot, S. L. and Mukhopadhyay, R. Dynamics of 1,3-Butadiene
636 Adsorbed in Na-Y Zeolite: MD Simulation Study, *Phys. Rev. E*, **2008**, *77*, 061201.

637 [30] Sharma, V. K., Gautam, S., Mitra, S., Rao, M. N., Tripathi, A. K., Chaplot, S. L. and
638 Mukhopadhyay, R., Dynamics of Adsorbed Hydrocarbon in Nanoporous Zeolite Framework, *J.*
639 *Phys. Chem. B*, **2009**, *113*, 8066-8072.

640 [31] Gautam, S. 'Use of Quasielastic Neutron Scattering and Molecular Dynamics Simulation to
641 Study Molecular Dynamics under Confinement' In *Horizons in World Physics*, Vol. 290,
642 Reimer, A. (Ed.), Nova **2017**, 25-44.

643 [32] Gautam, S., Ok, S., and Cole, D. R. Structure and Dynamics of Confined C-O-H Fluids
644 Relevant to the Subsurface: Application of Magnetic Resonance, Neutron Scattering and
645 Molecular Dynamics Simulations, Front. In Earth Sc. **2017** 5:43. doi: 10.3389/feart.2017.00043

646 [33] Papadopoulos, G. K., Jobic, H., and Theodorou, D. N. Transport Diffusivity of N_2 and CO_2
647 in Silicalite: Coherent Quasielastic Neutron Scattering Measurements and Molecular Dynamics
648 Simulations, *J. Phys. Chem. B*, **2004**, *108*, 12748 – 12756.

649 [34] Bui T., Phan A., Cole D. R., Striolo A. Transport Mechanism of Guest Methane in Water-
650 Filled Nano-Pores. *J. Phys. Chem. C* **2017**, *121*, 15675 – 15686.

651 [35] Argyris D., Cole D. R., Striolo A. Ion-specific Effects under Confinement: The Role of
652 Interfacial Water. *ACS Nano*. **2010,** *4*, 2035 – 2042.

653 [36] Le, T., Striolo, A., and Cole, D. R. Propane Simulated in Silica Pores: Adsorption
654 Isotherms, Molecular Structure, and Mobility, *Chem. Eng. Sci.* **2015**, *121*, 292-299.

655 [37] Ho, T. A., Argyris, D., Papavassiliou, D. V., Striolo, A., Lee, L. L. and Cole, D. R.
656 Interfacial Water on Crystalline Silica: A Comparative Molecular Dynamics Simulation Study
657 *Mol. Simu.* **2011**, *37*, 172-195.

658 [38] Martin, M. G. and Siepmann, J. I., Transferable Potentials for Phase Equilibria. 1. United
659 Atom Description of n-Alkanes, *J. Phys. Chem. B* **1998**, *102*, 2569 – 2577.

660 [39] Allen, M. P. and Tildesley, D. J. Computer Simulation of Liquids; Clarendon Pr.: Oxford,
661 **2004**.

662 [40] Berthelot, D. Sur Le Mélange Des Gaz. Comptes rendus hebdomadaires des séances de
663 l'Académie des Sciences, **1898**, 1703-1855.

664 [41] Lorentz, H. A. Ueber Die Anwendung Des Satzes Vom Virial in Der Kinetischen Theorie
665 Der Gase. *Annalen der Physik,* **1881**, *248*, 127-136.

666 [42] Cygan, R. T., Liang, J.-J. and Kalinichev, A. G. Molecular Models of Hydroxide,
667 Oxyhydroxide, and Clay Phases and the Development of a General Force Field. *J. Phys Chem. B*
668 **2004**, *108*, 1255-1266.

669 [43] Hoover, W. G. Canonical Dynamics: Equilibrium Phase-Space Distributions. *Phys. Rev. A*
670 **1985**, *31*, 1695-1697.

671 [44] Nosé, S. A Molecular Dynamics Method for Simulations in the Canonical Ensemble. *Mol.*
672 *Phys.* **1984**, *52*, 255-268.

673 [45] Essmann, U., Perera, L., Berkowitz, M. L., Darden, T., Lee, H. and Pedersen, L. G. A
674 Smooth Particle Mesh Ewald Method. *J. Chem. Phys* **1995**, *103*, 8577-8593.

675 [46] Hess, B., Kutzner, C., van der Spoel, D. and Lindahl, E. Gromacs 4: Algorithms for Highly
676 Efficient, Load-Balanced, and Scalable Molecular Simulation. *J. Chem. Theory Comput*. **2008**, *4*,
677 435-447.

678 [47] Van Der Spoel, D. Lindahl, E. Hess, B. Groenhof, G. Mark, A. E. and Berendsen, H. J. C.
679 Gromacs: Fast, Flexible, and Free. *J. Comput. Chem.* **2005**, 26, 1701-1718.

680 [48] Hockney, R. W., Goel, S. P., and Eastwood, J. W. Quiet High-Resolution Computer Models
681 of a Plasma. *J. Comput. Phys.* **1974**, *14*, 148-158.

682 [49] Gautam, S., Liu, T., Patankar, S., Tomasko, D., Cole, D. R. Location Dependent
683 Orientational Structure and Dynamics of Ethane in ZSM5, *Chem, Phys. Lett.* **2016**, *648*, 130 –
684 136.

685 [50] Choi, J.-G., Do, D. D., Do, H. D., Surface Diffusion of Adsorbed Molecules in Porous
686 Media: Monolayer, Multilayer, and Capillary Condensation Regimes, *Ind. Eng. Chem. Res.*
687 **2001**, *40*, 4005 – 4031.

688 [51] Gautam, S., and Cole, D., Molecular Dynamics Simulation Study of Meso-Confined
689 Propane in TiO_2, *Chem. Phys.* **2015**, *458*, 68 – 76.

690 [52] Argyris, D., Tummala, N. R., Striolo, A. and Cole, D. R., Molecular Structure and
691 Dynamics in Thin Water Films at the Silica and Graphite Surfaces, *J. Phys. Chem. C* **2008** *112*,
692 13587-13599.

693 [53] Tummala, N. R., Liu, S., Argyris, D. and Striolo, A., Interfacial Water Properties in the
694 Presence of Surfactants, *Langmuir* **2015,** *31*, 2084-2094

695 [54] Jobic, H., Bee, M., Kearly, G. J. Dynamics of ethane and propane in zeolite ZSM-5 studied
696 by quasielastic neutron scattering, *Zeolites*, **1992**, *12*, 146-151.

697 [55] Berne, B. J.; Pecora, R. Dynamic Light Scattering; John Wiley: New York, **1976**.